Electronic Supplementary Material (ESI) for Nanoscale.

Electronic Supporting Information

Tandem catalysis in multicomponent solvent-free biofluids

Dylan L. Atkins, José A. Berrocal, Alexander F. Mason, and Ilja K. Voets**

Table of Contents

1. Biohybrid Synthesis

1.1. Schematic representation of charge-stabilized biohybrid

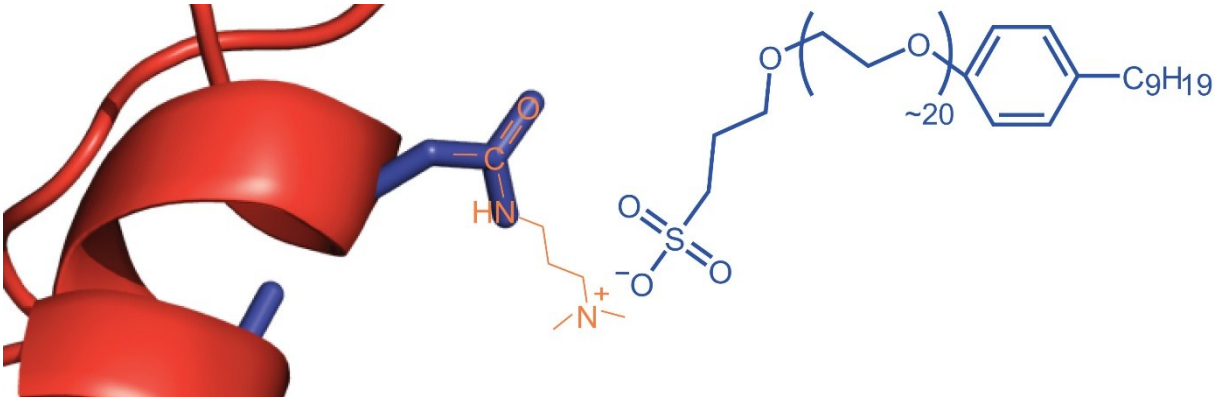

Figure S1. Anionic polymer surfactant poly(ethylene glycol)-4-nonylphenyl-3-sulfopropyl ether (S_1, depicted in blue) is electrostatically coupled to the solvent-accessible acidic residue Asp132 of Horseradish peroxidase. Charge-stabilized coupling is achieved via EDC-mediated cationization of solvent-accessible acidic residues with 3-(dimethylamino)-1-propylamine (depicted in orange).

1.2. Estimation of cationization efficiencies

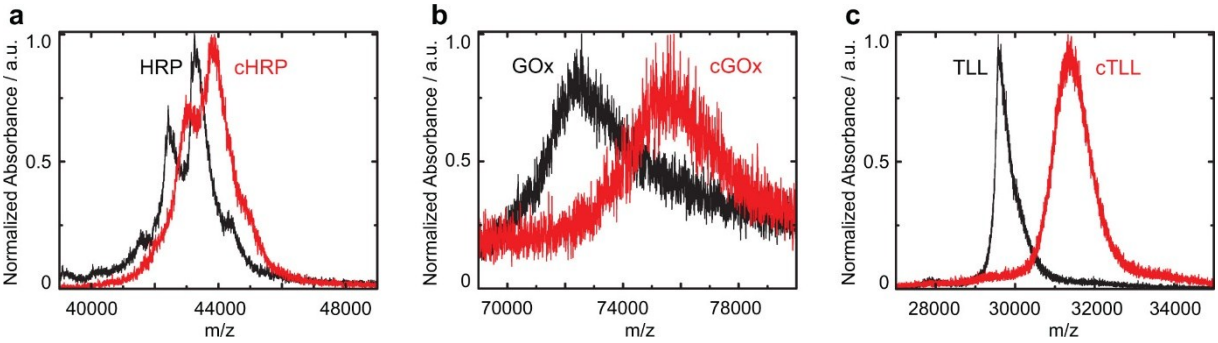

Figure S2**.** MALDI-TOF mass spectrometry profiles of (black) native and (red) supercharged variants of (a) horseradish peroxidase (HRP), (b) GOx, and (c) TLL. Acidic residue modification efficiencies of 78 %, 97 %, and 80 % were estimated for cationized HRP (cHRP), cationized GOx (cGOx), and cationized TLL (cTLL), respectively, from the observed shifts in peak maxima.

2. Computational Methods

2.1. Protein solvation

The location of specific enzymatic hydration waters was predicted using the Hypred[1] online tool and pdb files for horseradish peroxidase, glucose oxidase and Thermomyces lanuginosus lipase (TLL) (1hch, 1cf3 and 1ein, respectively).[2–4] Specifically, these were performed with H atoms included, and by excluding water cavities (potential water clusters which are enclosed by the protein). For all calculations a density cutoff of 1.1 e^{-} $Å^{-3}$ is applied. The predicted number of waters/enzyme were 1398 (HRP), 5183 (GOx), and 1194 (TLL).

2.2. Protein surface electrostatics

Continuum electrostatics calculations were performed using the PDB2PQR[5] webserver. The associated pdb file for HRP was supplied as an input for calculations, while a modified version for cHRP was prepared through mutagenesis of solvent-accessible Glu/Asp residues in PyMOL and by approximating these surface modifications as Lys residues. Initial calculations were performed using an AMBER forcefield and protonation states were assigned for pH 6.5. The resulting PQR files were used with default input parameters in the Adaptive Poisson-Boltzmann Solver (APBS)[6] to determine surface electrostatic parameters. The corresponding surface electrostatic potential maps could be visualized in PyMOL and were contour colored (red to blue) from -10 to +10 kT e^{-1}.

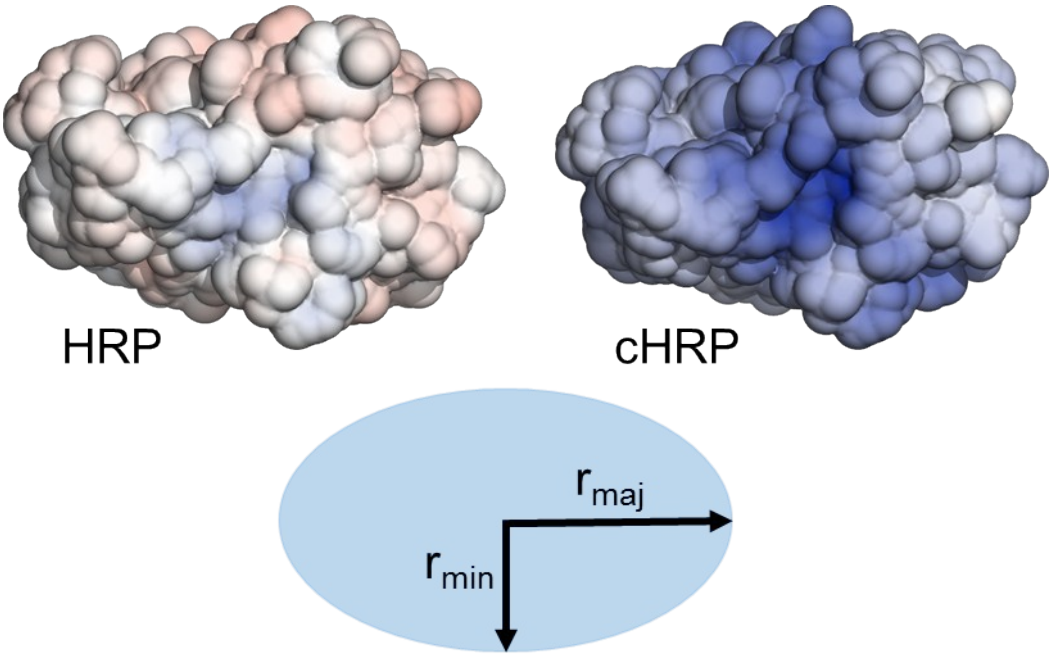

Figure S3. Map of surface electrostatic potential for horseradish peroxidase and supercharged variant. Electrostatic potentials for horseradish peroxidase (HRP) and cationized HRP (cHRP) are contour colored (red to blue) from -10 to +10 kT e^{-1}. The color map indicates the supercharged cHRP surface consists of patchy regions of high cationic charge density on the minor axis, with relatively neutral charge densities at the major axis extremities.

3. Biohybrid Synthesis

3.1. Thermogravimetric analysis

Thermogravimetric analysis was performed on a TA Instruments Q500 under N_2 flow. A heating ramp of 10 °C min^{-1} was performed between 25 – 600 °C, and the sample was incubated for 1 hr at 80 °C and again at 110 °C to remove atmospheric and specifically bound waters, respectively. This ensures that atmospheric waters which are re-absorbed after lyophilization are not misinterpreted as specifically bound. The mass loss after 1 hr at 110 °C was used to estimate the number of waters retained per protein-polymer hybrid after freeze-drying, while the mass remaining is the total mass of solvent-free protein-polymer hybrid. An example calculation for cHRP-S_1 is as follows,

Initial Mass	4.076 mg
Mass @ 109 °C	4.010 mg
Mass after incubation (110 °C, 1 hr)	4.000 mg
Mass of Specifically Bound Waters	0.010 mg
Moles of H_2O	5.61×10^{-7}
Moles of cHRP-S_1	5.97×10^{-8}
H_2O / cHRP-S_1 (mol/mol)	9.4 waters/hybrid

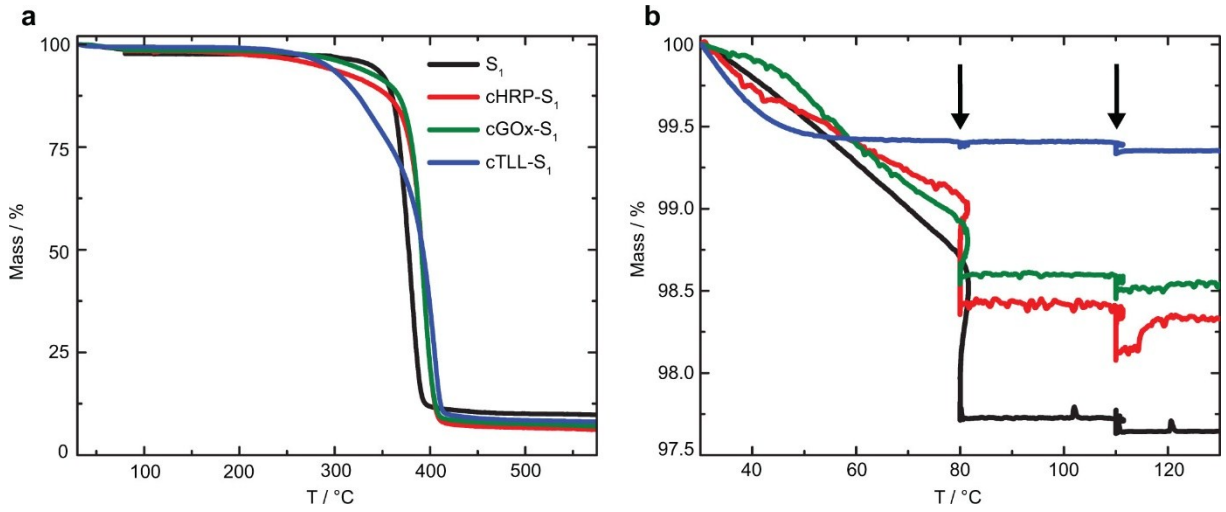

Figure S4. Thermal traces of neat S_1 (black), cHRP-S_1 (red), cGOx-S_1 (green) and cTLL-S_1 (blue) are shown from (a) 30 °C to 570 °C, or the same experiments on a reduced temperature scale from (b) 30 °C to 130 °C. Samples were subjected to the following thermal treatment: (1) ~6 min heating from room temperature to 80 °C at a constant heating rate of 10 °C min^{-1}, (2) incubation for 1 hr at 80 °C to liberate atmospheric waters (indicated by black arrow), (3) 3 min heating from 80 °C to 110 °C at a constant heating rate of 10 °C min^{-1}, (4) incubation for 1 hr at 110 °C to liberate specifically bound waters (indicated by black arrow), and (5) 49 min heating from 110 °C to 600 °C at a constant heating rate of 10 °C min^{-1}. The number of specifically bound waters per biohybrid is determined on a mol/mol basis using the mass loss over the 1 hr incubation at 110 °C, where the remaining mass of sample is the total mass of biohybrid.

3.2. Differential scanning calorimetry

Differential scanning calorimetry experiments were performed on a TA Instruments Q2000. Samples were first incubated at 80 °C to remove thermal history and cooled at 10 °C min^{-1} to -60 °C. Thermal cycles were subsequently performed between -60 °C to +80 °C at a constant temperature gradient of 10 °C min^{-1}. At least 2 cycles were performed to ensure sample phase behavior was unchanged over multiple thermal cycles.

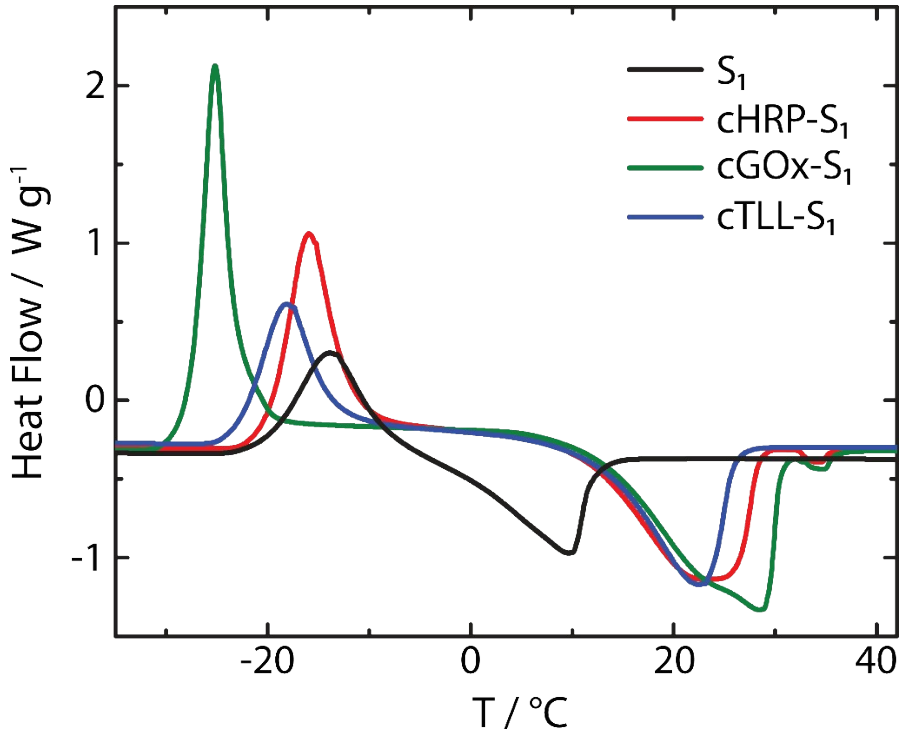

Figure S5. Differential scanning calorimetry of neat S_1 (black) and respective biohybrids cHRP-S_1 (red), cGOx-S_1 (green), and cTLL-S_1 (blue). Samples are initially heated to +80 °C to remove thermal history, and then subjected to 2 complete cooling and heating cycles from +80 °C to -60 °C at a constant heating/cooling rate of 10 °C min^{-1}. Only the second of the complete heating cycles is shown here from -30 °C to 42 °C.

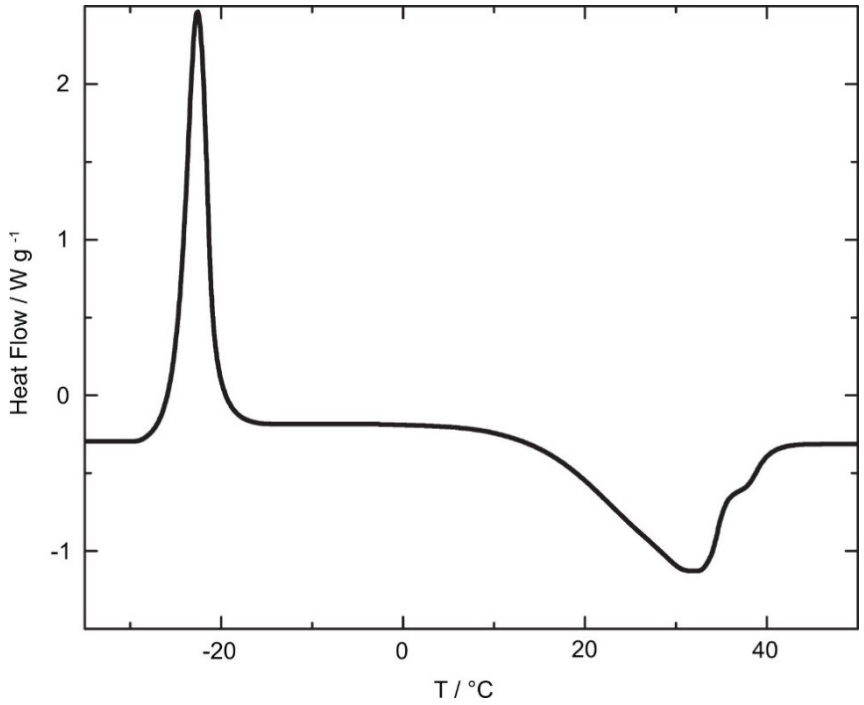

Figure S6. Differential scanning calorimetry of cGOx-S_1/cHRP-S_1 mixed enzyme biofluid. The sample is initially heated to +80 °C to remove thermal history, and then subjected to 2 complete cooling and heating cycles from +80 °C to -60 °C at a constant heating/cooling rate of 10 °C min^{-1}. Only the first of the complete heating cycles is shown here from -35 °C to 50 °C. A distinct melting transition is shown to exist at 32 °C.

3.3 Optical microscopy

We first aimed to probe the miscibility of small amounts of neat desiccated OPD or glucose substrates under thermal annealing at 110 °C in the single component cHRP-S_1 melt using optical microscopy. Significantly, this was performed above the melting point of OPD (98-102 °C) and below that of glucose (150-152 °C), respectively. Under simulated reaction conditions we observed the initial melting of OPD followed by rapid diffusion throughout the solvent-free biofluid (Figure S7). Further, solubilization at the solid-liquid interface of glucose crystals is observed over approximately 70 s, whereby no further glucose crystals are observable by microscopy (Figure S8).

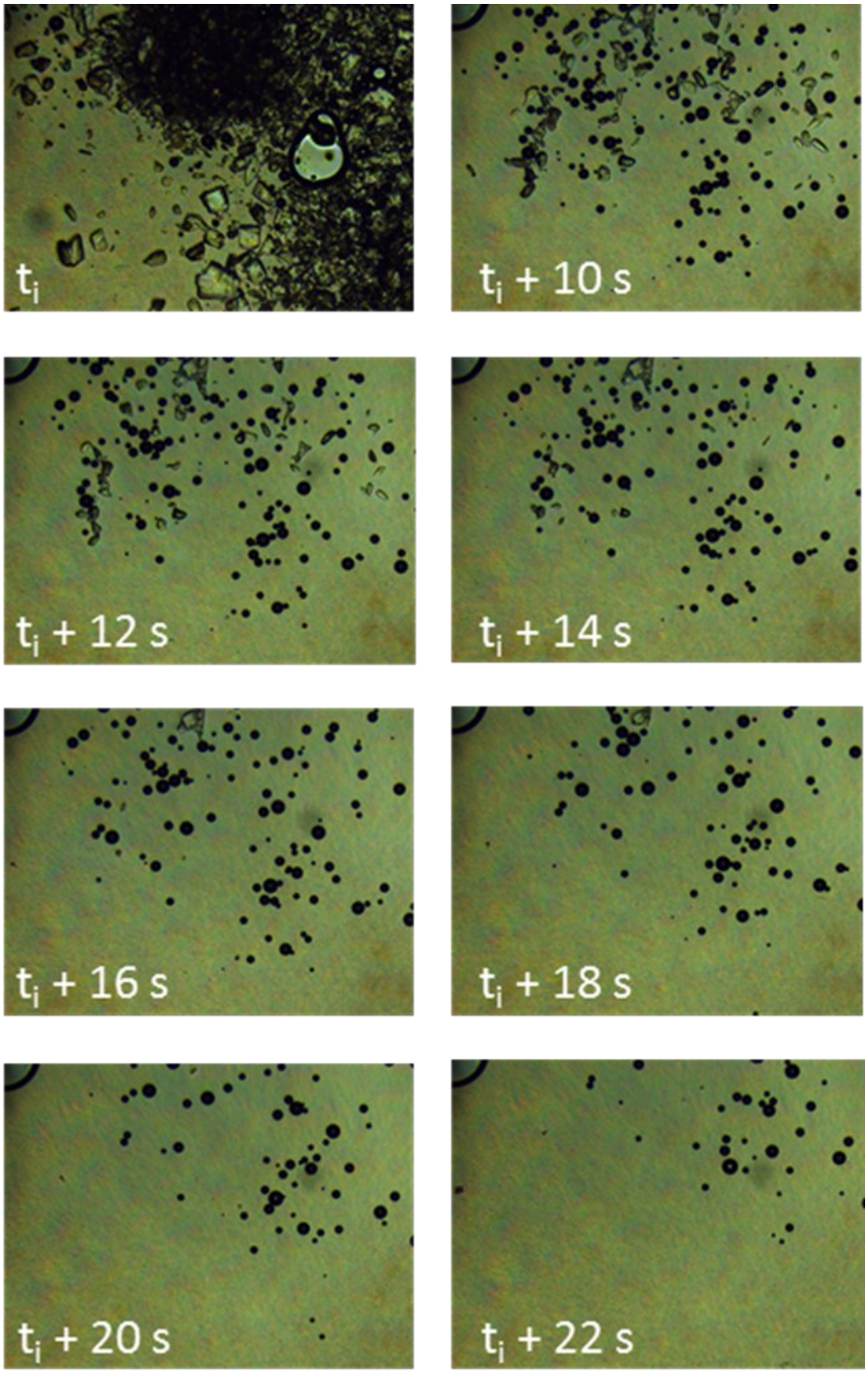

Figure S7. Optical microscopy images show the initial melting of OPD crystals (at time t_i) into dark droplets which are readily miscible with the solvent-free biofluid and diffuse freely at 110 °C.

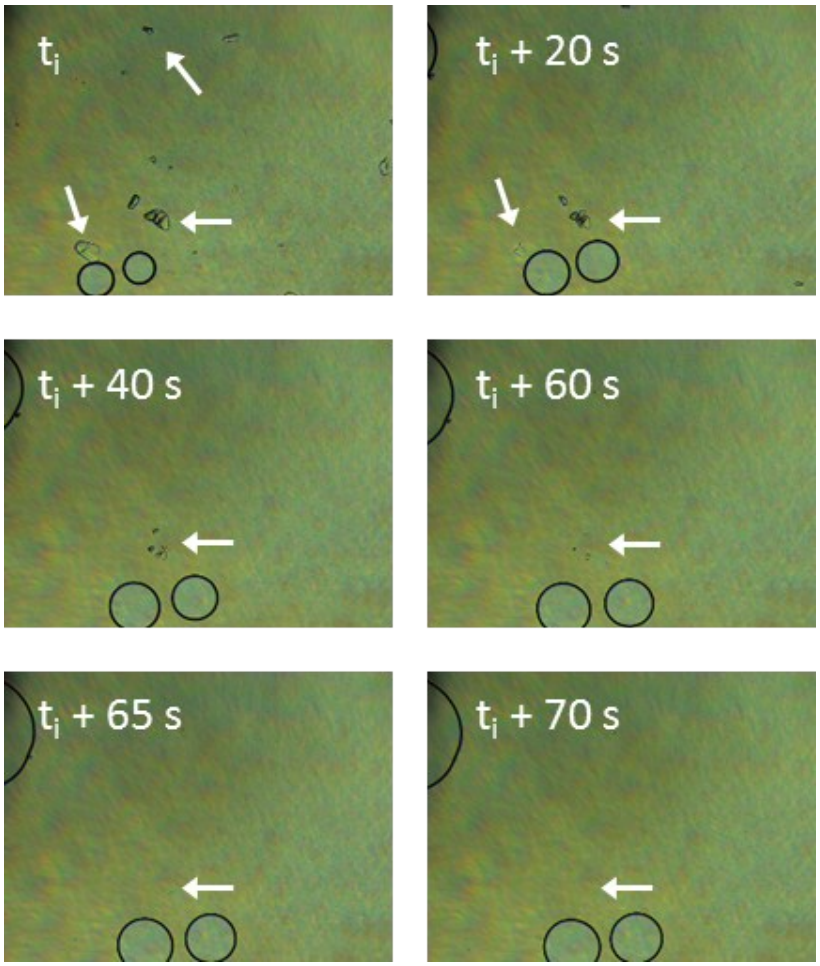

Figure S8. Optical microscopy images show solubilization at the solid-liquid interface of glucose crystals by the solvent-free biofluid over approximately 70 s at 110 °C.

3.4. Temperature-dependent rheology

Rheology experiments to determine the temperature-dependent viscosity were performed on an Anton Paar Physica MCR 301. A parallel plate geometry (7.95 mm diameter) was used with applied shear rates ranging from 0.1 – 10 s^{-1}, and a constant gap of 0.15 mm. Experiments were performed over a range of 40 – 150 °C at 10 °C intervals. Substrate diffusion coefficients were subsequently determined using the Stokes-Einstein relation,

$$q = \frac{kT}{6\pi\eta r}$$

where D is the diffusion coefficient ($cm^2\ s^{-1}$), k is the Boltzmann constant, η is the viscosity of the protein-polymer biofluid (Pa s), and r is the substrate radius (cm), being 1 Å for H_2O_2.

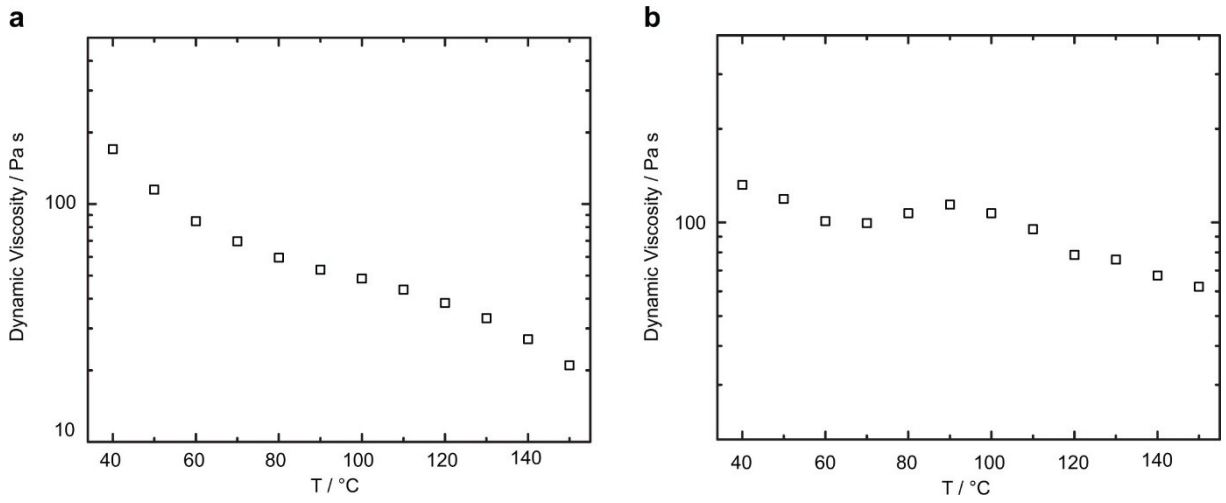

Figure S9. (a) Dynamic viscosity versus temperature of the cGOx-S_1/cHRP-S_1 reaction mixture from 40 °C to 150 °C at 10 °C intervals. (b) Dynamic viscosity versus temperature of the cTLL-S_1/cGOx-S_1/cHRP-S_1 reaction mixture from 40 °C to 150 °C at 10 °C intervals.

4. Small-Angle X-Ray Scattering Analysis

4.1. Ellipsoidal form factor

Table S1. Ellipsoidal form factor fit parameters of horseradish peroxidase (HRP) and cationized HRP (cHRP) using SasView.

	HRP	**cHRP**
Background (cm^{-1})	2.45e-04	2.65e-04
R_{min} (Å)	18.18	18.53
R_{max} (Å)	32.89	33.22
Volume Fraction	0.0049	0.0049
SLD_{ell} ($Å^{-2}$)	8.76e-06	8.76e-06
SLD_{sol} ($Å^{-2}$)	9.46e-06	9.46e-06

4.2. Core-shell ellipsoidal form factor

Table S2. Core-shell ellipsoidal form factor fit parameters of biohybrid cHRP-S_1 using SasView.

	cHRP-S_1
Background (cm^{-1})	1.03e-04
$R_{min,core}$ (Å)	18.53
$R_{min,shell}$ (Å)	49.64
$R_{max,core}$ (Å)	33.22
$R_{max,shell}$ (Å)	38.22
Volume Fraction	0.0024
SLD_{ell} ($Å^{-2}$)	8.76e-06
SLD_{shell} ($Å^{-2}$)	9.28e-06
SLD_{sol} ($Å^{-2}$)	9.46e-06

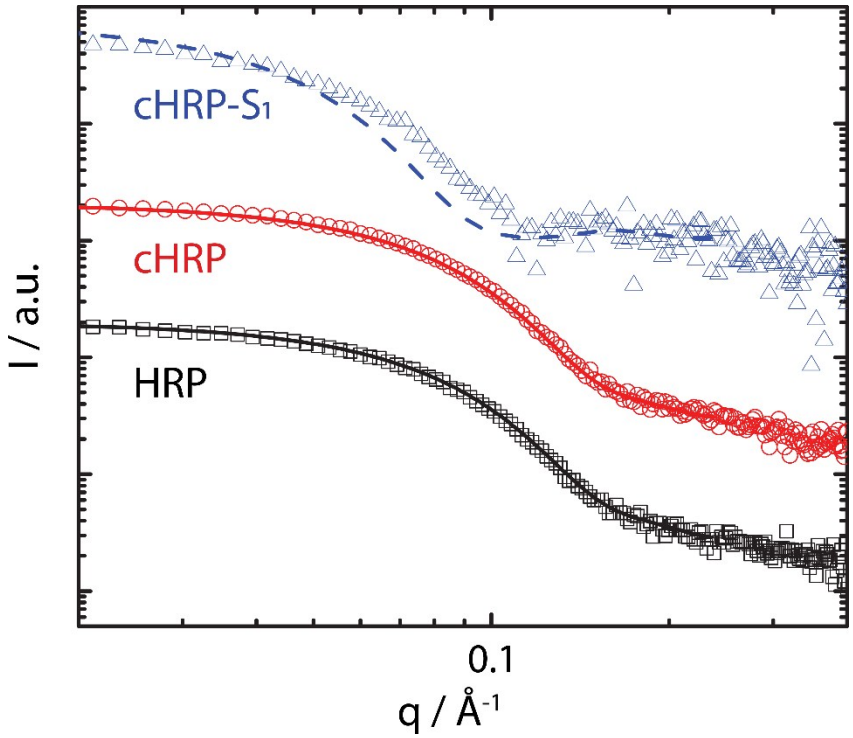

Figure S10. Solution state SAXS profiles of native HRP (black), supercharged cHRP(red), and biohybrid cHRP-S_1 (blue) variants. Corresponding ellipsoidal form factor fits are shown for HRP (black) and cHRP (red). An example of a poor cHRP-S_1 fit using a core-shell ellipsoidal form factor with homogenous shell thickness (3.1 nm, blue dashed line) is indicated.

5. Kinetics of Biohybrids

5.1. cHRP-S1 kinetic assays

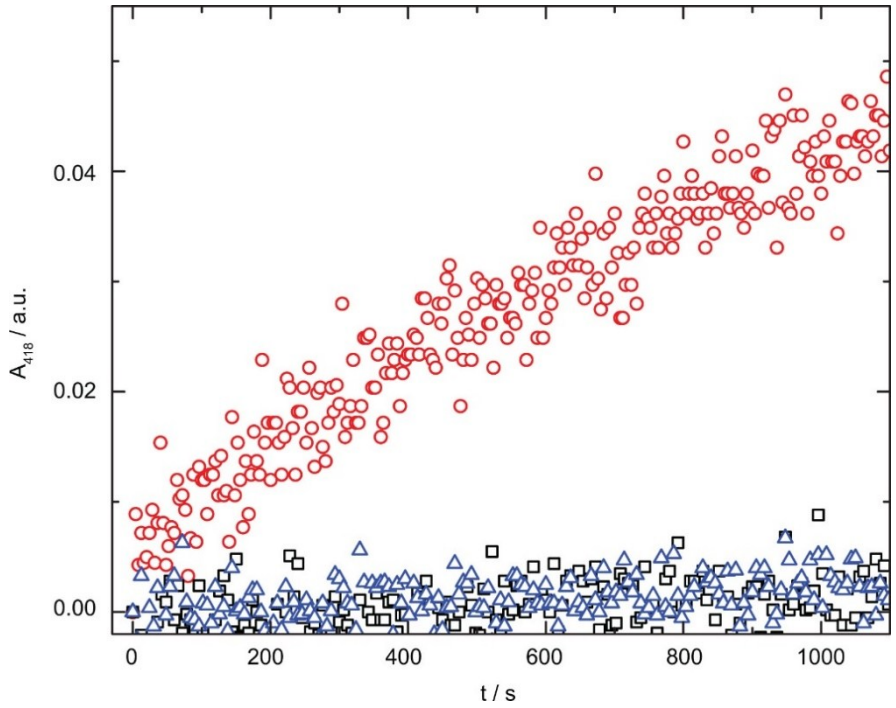

Figure S11. The solvent-free cHRP-S_1 catalyzed conversion of *o*-phenylenediamine (OPD) into 2,3-diaminophenazine (DAP) was determined photospectroscopically by monitoring the DAP absorbance at $\lambda = 418$ nm and 2 second time intervals during 20 minutes. OPD is rapidly converted into DAP in the cHRP-S_1 melt at 90 °C and in the presence of H_2O_2 (red squares) as evidenced by a significant increase in absorption. Control experiments in the cHRP-S_1 melt without H_2O_2 (black squares) or in neat S_1 (blue diamonds) at 110 °C show that auto-oxidation of OPD is negligible, and that cHRP is essential for the catalytic turnover of OPD into DAP.

5.2. Low-temperature cGOx-S1/cHRP-S1 kinetic assays

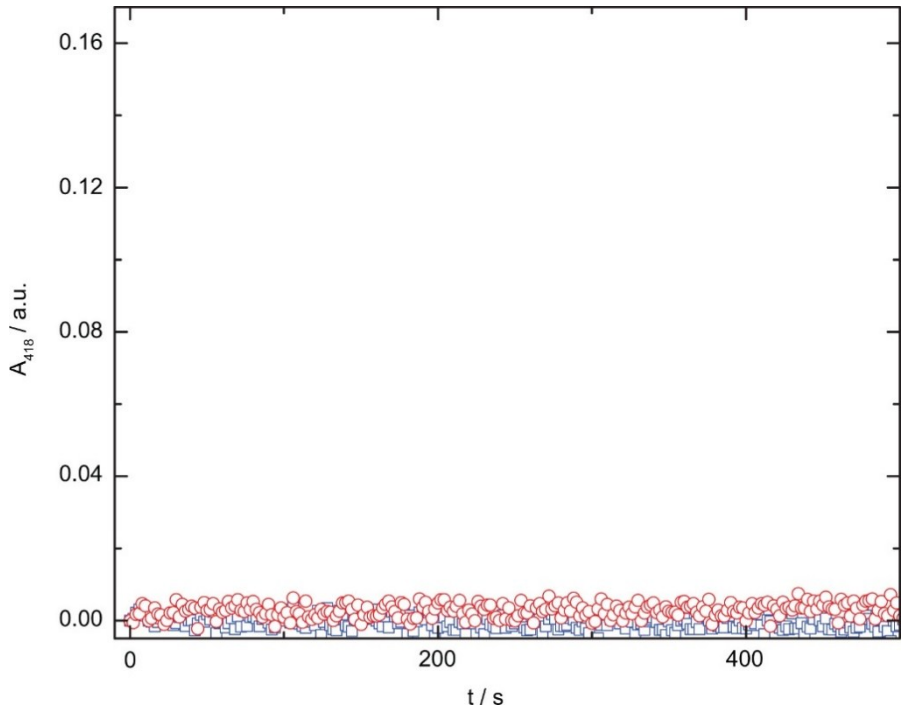

Figure S12. Control experiments of the cGOx-S_1/cHRP-S_1 mixed enzyme biofluid in the presence of *o*-phenylenediamine (OPD) and glucose at 40 °C (blue squares) or 60 °C (red circles). The lack of change in absorbance at λ = 418 nm over 500 s indicates that 2,3-diaminophenazine (DAP) is not produced, and an apparent thermal threshold for catalytic activity exists.

5.3. Multicomponent biofluid activity over elaborate time periods

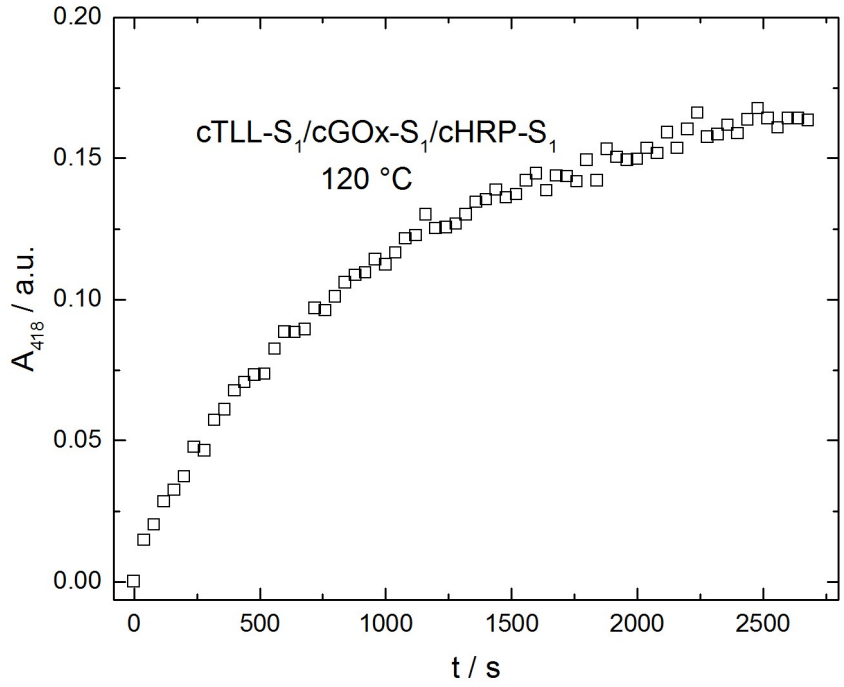

Figure S13. Absorbance at 418 nm versus time indicating the production of DAP at 120 °C within the cTLL-S_1/cGOx-S_1/cTLL-S_1 biofluid over an elaborate time period. For clarity every 20th data point is plotted.

6. Synthesis and Characterization of Carboxylated Brij® L23 (S_6)

Unless otherwise stated all materials were purchased from Sigma-Aldrich, NL. The TEMPO-mediated oxidation of Brij® L23 was performed using a modified previously reported protocol.[7] In a single batch synthesis, Brij® L23 (10 g) was oxidized in water (100 mL) with TEMPO (Fluorochem, 286 mg), NaBr (286 mg), and 29 mL NaClO (available chlorine > 5.0 %) at pH > 10 for 24 hrs at room temperature. The oxidation was quenched by the addition of 30 mL of EtOH, followed by acidification with HCl to pH < 1 and three extractions with 100 mL aliquots of CH_2Cl_2. The combined CH_2Cl_2 layers were dried under reduced pressure and dissolved in 250 mL hot ethanol, followed by precipitation in a freezer overnight. Filtration of the waxy solid afforded 8.3 g of S_6.

^{1}H NMR (400 MHz, DMSO-d_6) δ: 12.60 (broad s, 1H), 4.01 (s, 2H), 3.51 (m, 90H), 1.47 (p, J = 8 Hz), 1.24 (m, 18H), 0.86 (t, J = 8 Hz, 3H). **^{13}C NMR** (100 MHz, DMSO-d_6) δ: 172.1, 72.83, 70.78, 69.96, 68.05, 60.69, 31.78, 29.69, 29.51, 29.49, 29.35, 29.19, 26.13, 19.02, 14.41. **FT-IR (ATR)** ν: 3476 (O-H, broad), 2884 (C-H, strong), 1744 (C=O, strong), 1107 (C-O-C, strong).

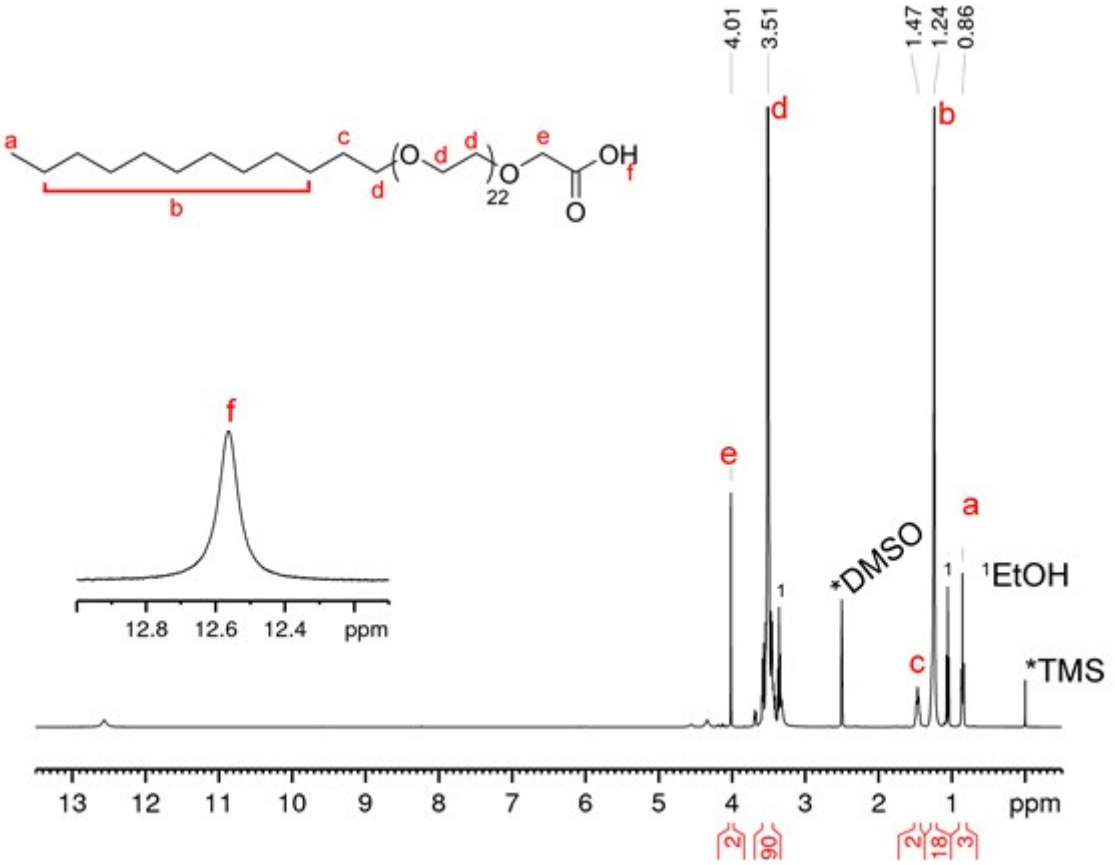

Figure S14. ^{1}H NMR (400 MHz, DMSO-d_6) spectrum of S_6. The inset in the 13.0-12.1 ppm region shows the broad singlet related to the carboxylic group.

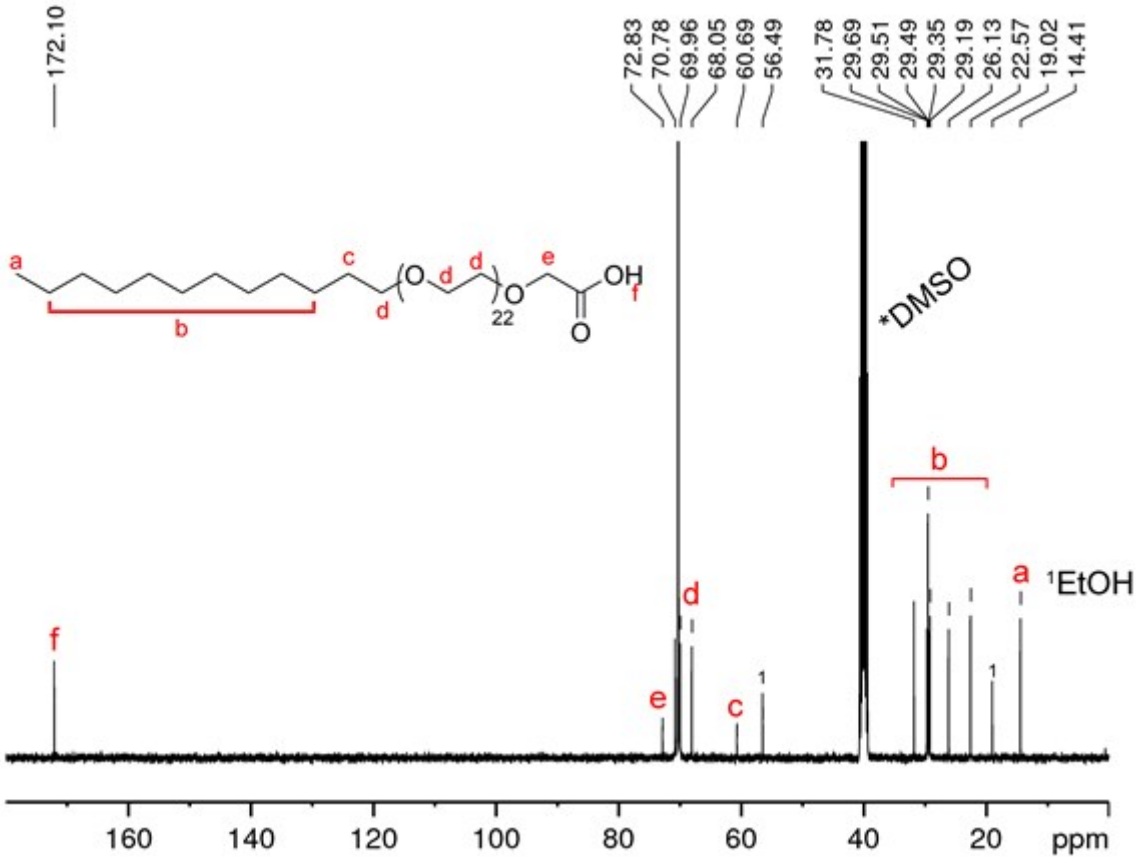

Figure S15. ^{13}C NMR (100 MHz, DMSO-d_6) spectrum of S_6.

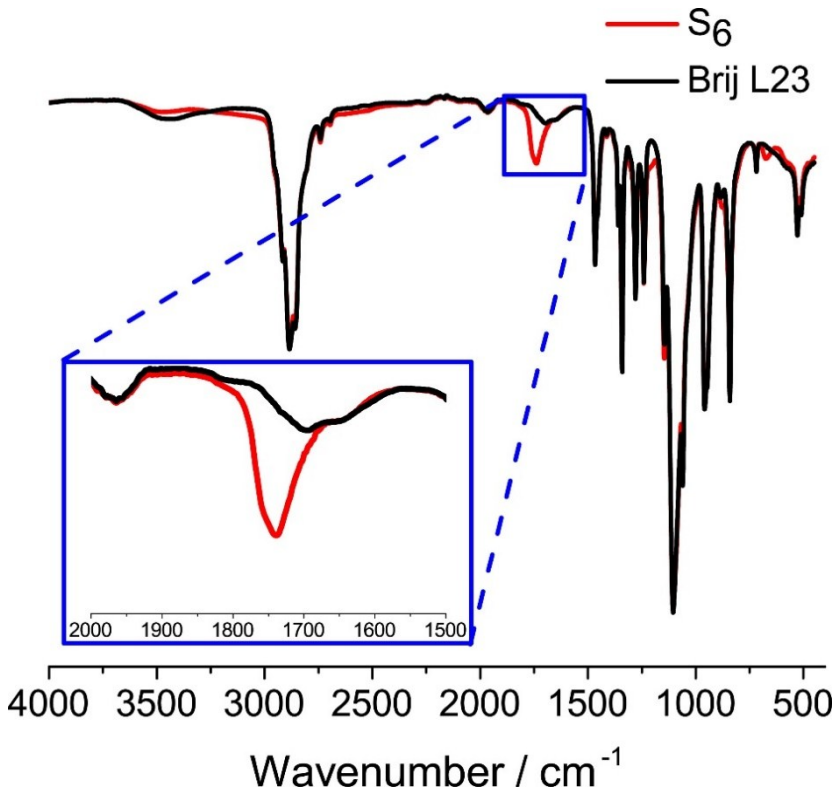

Figure S16. Overlapped FT-IR spectra of Brij 35 (black line) and S_6 (red line). The blue rectangle shows an expansion in the 2000-1500 cm^{-1} window, with the diagnostic –COOH vibration for S_6.

7. Synthesis and Characterization Acetylated Glucose (AcGl)

All chemicals were used as received unless otherwise stated, and were supplied by Sigma-Aldrich. Dry CH_2Cl_2 was obtained using an MBraun SPS-800 dry solvent system, with solvent dried over 2 columns of aluminium oxide. Triethylamine was dried over activated 4 Å molecular sieves. Column chromatography was performed using a Biotage Isolera One column robot.

NMR spectra were acquired using a Bruker Avance III 400 MHz spectrometer. Multiplicities are assigned as singlet (s), doublet (d), triplet (t), quartet (q), broad (br) or multiplet (m). Chemical shifts are measured in parts per million (ppm), internally referenced relative to TMS. Low resolution electron spray ionisation spectra (ESI) were acquired using a Thermo Scientific LCQ Fleet equipped with a Kinetex 5μm EVO C18 column (Phenomenex).

Synthesis of 1-*O*-acetyl-2,3,4,6-tetra-*O*-benzyl-d-glucopyranose

2,3,4,6-tetra-*O*-benzyl-d-glucopyranose (2.007 g, 2.71 mmol, 1 eq.) was transferred to a 250 mL 2-necked flask and dissolved in dry CH_2Cl_2 (70 mL). To this stirred solution was added dry triethylamine (544 μL, 3.90 mmol, 1.05 eq.), followed by acetic anhydride (369 μL, 3.90 mmol, 1.05 eq.). The reaction mixture was stirred under argon, at room temperature, for 2 hours, at which point another aliquot of both triethylamine (544 μL, 3.90 mmol, 1.05 eq.) and acetic anhydride (369 μL, 3.90 mmol, 1.05 eq.) were added and left to react overnight. The crude reaction mixture was washed with 1 M HCl (3 x 100 mL), saturated $NaHCO_3$ (2 x 100 mL), ultrapure water (1 x 100 mL), and brine (1 x 100 mL). The organic phase was dried over $MgSO_4$, concentrated *in vacuo*, and purified *via* silica chromatography (CH_2Cl_2) to yield **1-*O*-acetyl-2,3,4,6-tetra-*O*-benzyl-d-glucopyranose** (1.62 g, 75%) as a white solid. Characterization data are consistent with those previously reported in the literature.[8]

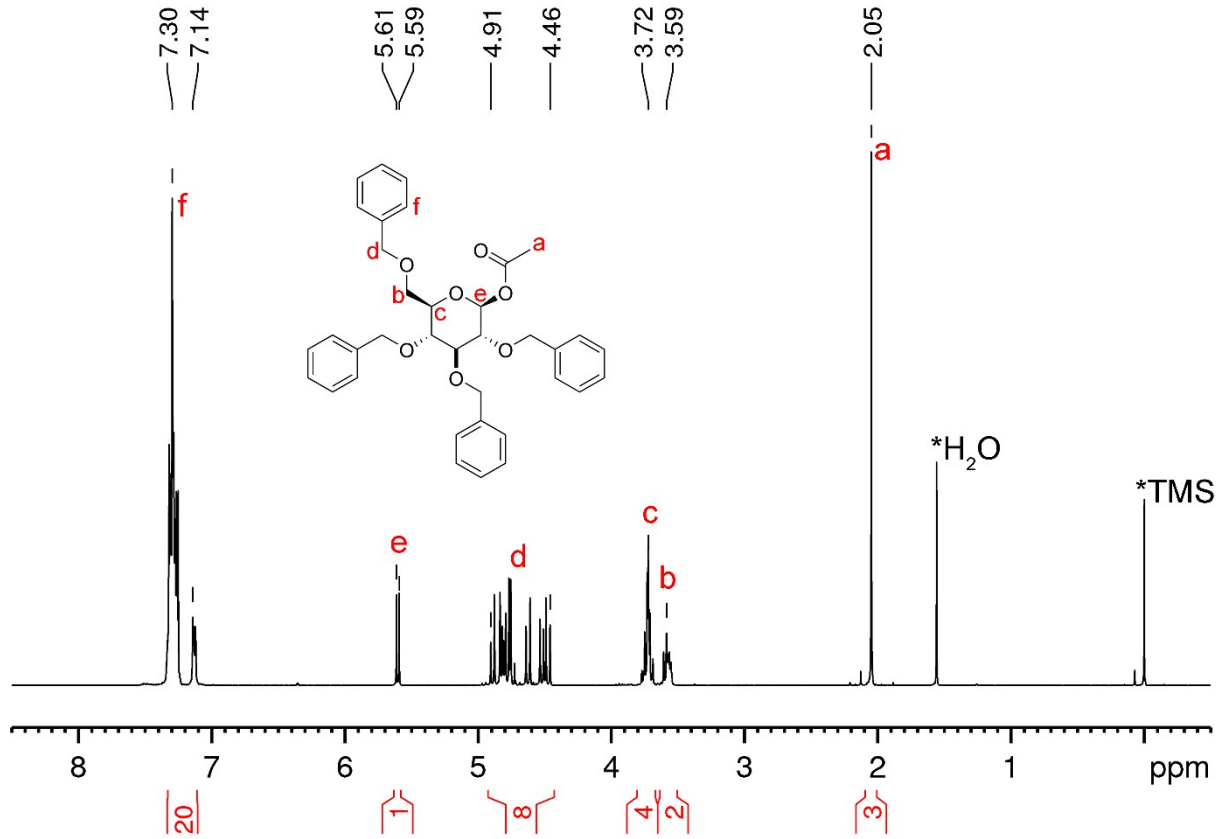

Figure S17. ^{1}H NMR of **1-*O*-acetyl-2,3,4,6-tetra-*O*-benzyl-d-glucopyranose** (400 MHz, $CDCl_3$) δ 7.35 – 7.26 (m, 18H), 7.16 – 7.10 (m, 2H), 5.60 (d, J = 8.1 Hz, 1H), 4.93 – 4.43 (m, 8H), 3.79 – 3.66 (m, 4H), 3.63 – 3.52 (m, 2H), 2.05 (s, 3H).

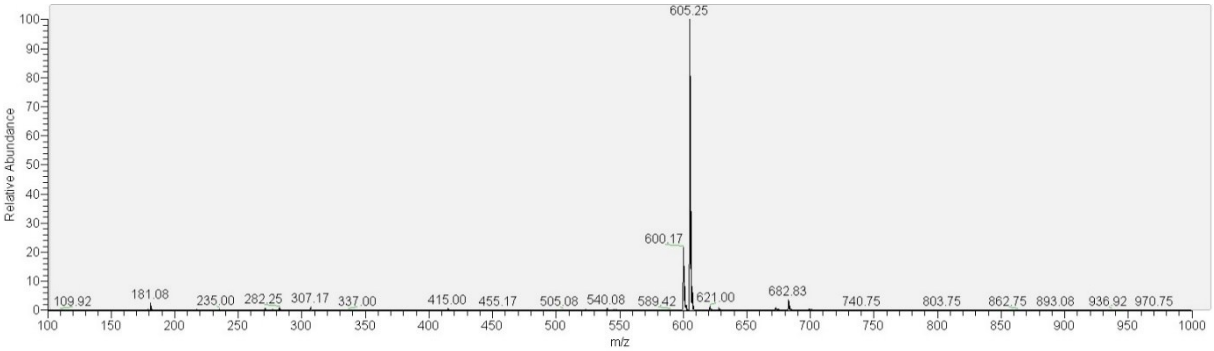

Figure S18. Mass spectrum of **1-*O*-acetyl-2,3,4,6-tetra-*O*-benzyl-d-glucopyranose** (ESI) *m/z* = 605.25 $[M+Na]^+$ (calculated = 605.25).

Synthesis of 1-*O*-acetyl-d-glucopyranose

1-*O*-acetyl-2,3,4,6-tetra-*O*-benzyl-d-glucopyranose (1.50 g, 2.58 mmol) was dissolved in a 2:1 mixture of methanol:ethyl acetate (60 mL). The solution was sparged for 15 minutes with argon, followed by the addition of a spatula tip of palladium on carbon (Degussa type E101, 10% loading on wet support). The reaction mixture was then sparged with hydrogen from a balloon for 15 minutes, and left to react at room temperature under a positive pressure of hydrogen overnight. The Degussa type Pd/C proved to be necessary to facilitate complete deprotection, as incomplete deprotection was observed using other types of Pd/C. The reaction mixture was filtered through a celite plug and concentrated *in vacuo* to yield **1-*O*-acetyl-d-glucopyranose** (0.52 g, 91%) as a waxy solid. These characterization data are consistent with those previously reported in the literature.[8]

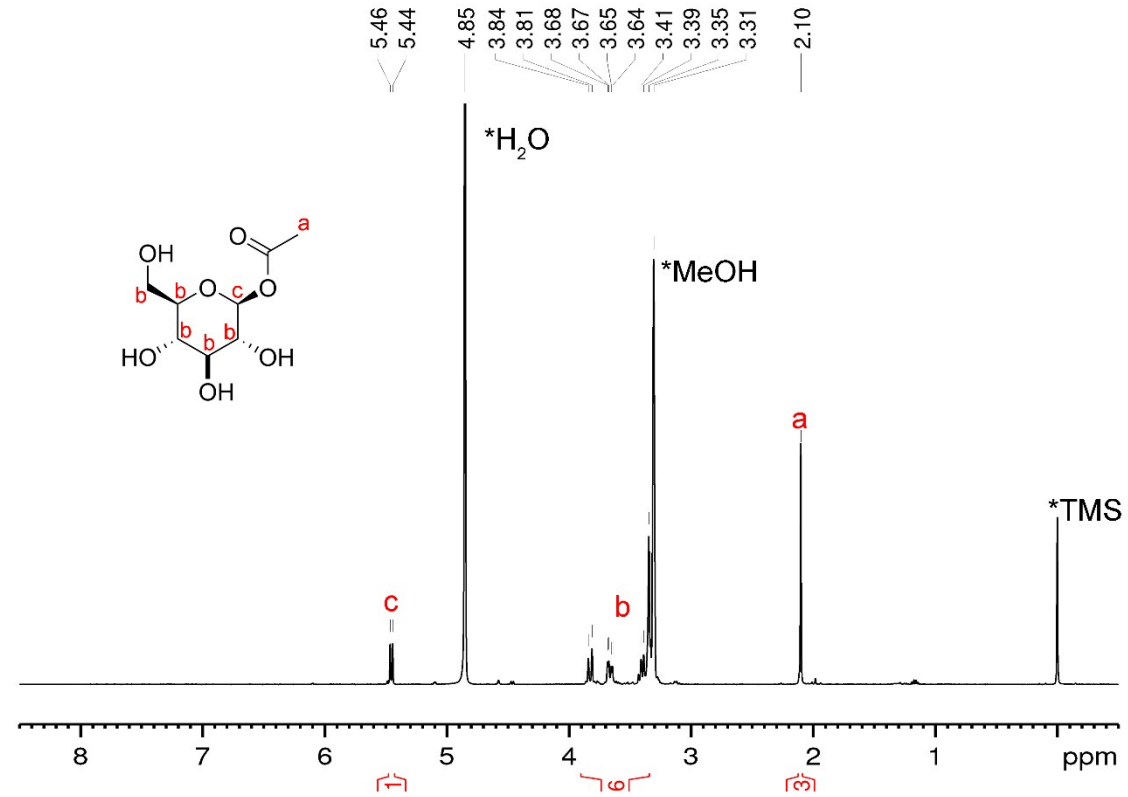

Figure S19. ^{1}H NMR of **1-*O*-acetyl-d-glucopyranose** (400 MHz, CD_3OD) δ 5.46 (d, J = 7.9, 1H), 3.91 – 3.24 (m, 6H), 2.10 (s, 3H).

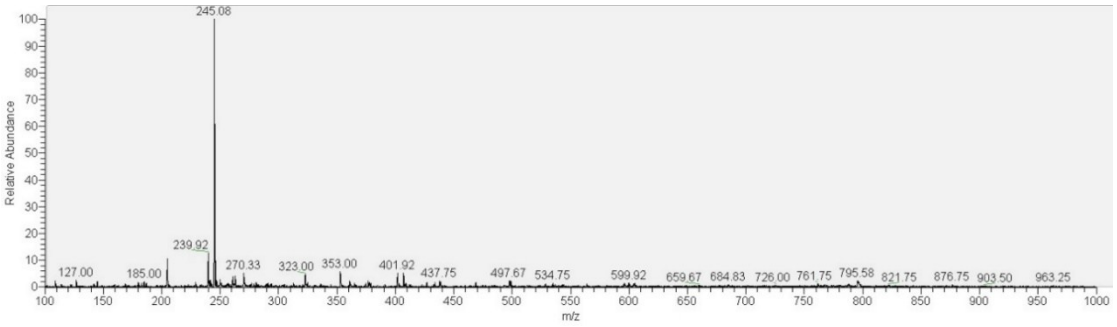

Figure S20. Mass spectrum of **1-*O*-acetyl-d-glucopyranose** (ESI) m/z = 245.08 $[M+Na]^+$ (calculated = 245.06).

Supplementary References

[1] J. J. Virtanen, L. Makowski, T. R. Sosnick, K. F. Freed, *Biophys. J.* **2010**, *99*, 1611.

[2] G. I. Berglund, G. H. Carlsson, A. T. Smith, H. Szöke, A. Henriksen, J. Hajdu, *Nature* **2002**, *417*, 463.

[3] G. Wohlfahrt, S. Witt, J. Hendle, D. Schomburg, H. M. Kalisz, H. J. Hecht, *Acta Crystallogr. D. Biol. Crystallogr.* **1999**, *55*, 969.

[4] A. M. Brzozowski, Hugh Savage, Chandra S. Verma, Johan P. Turkenburg, D. M. Lawson, A. Svendsen, P. Sham, *Biochemistry* **2000**, *39*, 15071.

[5] T. J. Dolinsky, J. E. Nielsen, J. A. McCammon, N. A. Baker, *Nucleic Acids Res.* **2004**, *32*, W665.

[6] N. A. Baker, D. Sept, S. Joseph, M. J. Holst, J. A. McCammon, *Proc. Natl. Acad. Sci.* **2001**, *98*, 10037.

[7] J. Araki, C. Zhao, K. Ito, *Macromolecules* **2005**, *38*, 7524.

[8] S. F. M. van Dongen, M. Nallani, J. J. L. M. Cornelissen, R. J. M. Nolte, J. C. M. van Hest, *Chem. - A Eur. J.* **2009**, *15*, 1107.